J Mater Sci (2010) 45:6747–6756
DOI 10.1007/s10853-010-4769-9

Synthesis of TiC from porous carbon coating on Si–C–O (Nicalon) fibres by reactive chemical vapour deposition in pressure-pulsed mode or at atmospheric pressure

I. Jouanny · S. Jacques · P. Weisbecker · C. Labrugère · M. Lahaye · L. Maillé · R. Pailler

Received: 1 February 2010 / Accepted: 13 July 2010 / Published online: 28 July 2010

Abstract TiC coatings were synthesised on NL202 Nicalon fibres through the treatment of a porous carbon coating at the surface of the fibres by thermal reactive chemical vapour deposition (RCVD) either in pressure-pulsed (P-RCVD) mode at low pressure or at atmospheric pressure (AP-RCVD) with a $H_2/TiCl_4$ gaseous mixture. The conversion rate of C into TiC was studied as a function of the $H_2/TiCl_4$ pulse number for the P-RCVD method and as a function of the treatment time for the AP-RCVD method. Chemical and micro-structural characterisations of the coatings were carried out by X-ray photoelectron spectroscopy, Auger electron spectroscopy and scanning and transmission electron microscopies. Mechanical assessment was achieved by tensile tests at room temperature. For the P-RCVD method, the conversion rate increased when the number of $H_2/TiCl_4$ pulses increased from 20 to 100. Once 20 $H_2/TiCl_4$ pulses were performed, an interlayer made of TiC was observed at the carbon coating/fibre interface indicating that the $H_2/TiCl_4$ gas has diffused inside the porous carbon and has reacted in depth and more particularly at the coating/fibre interface. With 100 pulses, the carbon coating was totally converted. For the AP-RCVD method, the conversion rate increased when the treatment time increased from 30 to 60 min. The reaction of conversion began preferentially at the outermost surface of the carbon coating but several isolated TiC grains were also observed at the coating/fibre interface. At atmospheric pressure, the gaseous mixture was more reactive than at low pressure whereas the diffusion of the gaseous species was limited inside the carbon coating. The mechanical properties of the fibre decreased when the conversion rate of the carbon into TiC increased both in P-RCVD and AP-RCVD.

I. Jouanny (✉) · S. Jacques · P. Weisbecker · L. Maillé · R. Pailler
Laboratoire des Composites Thermostructuraux, Allée de La Boétie, Université de Bordeaux1, CNRS, SPS, CEA, 33600 Pessac, France
e-mail: isabellejouanny@hotmail.fr

C. Labrugère · M. Lahaye
Centre de Caractérisation des Matériaux Avancés, 87 Avenue du Docteur Albert Schweitzer, 33608 Pessac, France

Introduction

Ceramic matrix composites (CMCs) are valuable materials for applications in severe conditions (high temperature, oxidising atmosphere, particle irradiation, etc.) such as turbine engine components, spacecraft thermal protection systems, nuclear energy devices, etc. [1, 2]. To improve the thermal–mechanical properties, an interphase with thickness ranging from 0.1 to 1 μm is inserted between the matrix and the fibre. The two main functions of this interphase are: (i) to realize a diffusion barrier in order to protect the fibre from oxidising atmospheres at high temperature and (ii) to act as a mechanical fuse, deflecting microcracks present in the matrix under mechanical solicitation while maintaining a good load transfer between matrix and fibres. These tasks are better fulfilled when the interphase is strongly bonded to the fibres [3].

Currently, the most common interphases found in CMCs are made of pyrocarbon (pyC). Indeed, pyC appears to be a good mechanical fuse, thanks to its lamellar structure and its synthesis is well controlled. However, pyC interphases are very sensitive to oxidation at temperatures as low as 400 °C. Furthermore, pyC undergoes an important anisotropic swelling under neutron irradiation that can be detrimental for nuclear applications. It is thus necessary to

find new and better interphases, without free carbon, in order to fulfil current and future industrial and environmental requirements. These interphases must be refractory, oxidation-resistant and chemically compatible with the constituents of the matrix and the fibre at high temperature.

Porous coatings have been proposed as an alternative to lamellar interphases in CMCs [3–7]. Indeed, the presence of porosity allows crack deflection. Carpenter et al. proposed to introduce a porous domain in between two dense layers; an outer one to avoid the filling of pores during the matrix deposition and an inner one to protect the fibres from oxidising species during the solicitation of the material [4]. Several ways to obtain porous interphases are possible. Porous oxide interphases can be synthesised through burning of an oxide/carbon coating deposited at the fibre surface. During this step, the carbon is removed and a porous system is created in the place of the fugitive carbon [3]. Such concepts were studied and validated experimentally in all-oxide composites [5, 6]. Finally, SiC-based CMCs with a porous interphase derived from Al_2O_3/SiO_2 have been also prepared through the sol gel process [7]. Two kinds of coatings were obtained: one consisting of a micro- (fibre side) and meso-porous (matrix side) double-layer and the other one consisting of a macroporous single-layer. SiC/SiC microcomposites with such Al_2O_3/SiO_2 porous interphases had high tensile strengths, around 1,050 MPa, despite a brittle behaviour.

The aim of this article was to obtain a nanoporous titanium carbide interphase on the surface of SiC-based fibres by means of a new two-step process. The first step lies in using Gogotsi's method [8], e.g. using a chlorine treatment to form a porous carbon coating at the surface of the fibre. During the second step, this porous carbon coating is converted into a TiC coating by thermal reactive chemical vapour deposition (RCVD) with a H_2/$TiCl_4$ gaseous mixture [9, 10]. Each method allows adherent, homogeneous and thin coatings to be obtained. Hence, if the initial carbon coating porosity was kept during the RCVD conversion into TiC, a porous carbide layer would be achieved for application as an interphase in CMCs.

Experimental

Synthesis of coatings

The SiC-based fibres used in this study were NL202 Nicalon fibres (~14 μm in diameter, from Nippon Carbon, Japan). The porous carbon coatings were first obtained at the fibre surface through a chlorination treatment according to the process detailed by Delcamp et al. [11]. The thickness and the pore-size of the porous carbon coatings were about 200 and 0.8 nm, respectively.

Then, the porous carbon coatings were converted into TiC coatings by RCVD with a H_2/$TiCl_4$ gaseous mixture according to the following equation:

$$C(s) + TiCl_4(g) + 2H_2(g) = TiC(s) + 4HCl(g). \quad (1)$$

In this case, TiC was formed by a heterogeneous reaction between the carbon of the initial porous coating and the $TiCl_4$ gas. The reactor used in this work was a silica tube with an inner diameter of 6 cm. The hot area of the reactor was about 10 cm in length. The silica tube was placed inside a conventional electrical resistive furnace. Two variants of RCVD were used: a pressure-pulsed RCVD method at low pressure (P-RCVD) and a RCVD method at atmospheric pressure (AP-RCVD). Table 1 lists the main synthesis parameters of the TiC coatings obtained with both RCVD variants that are described in details below.

The P-RCVD variant is a combination of the RCVD method with a pressure-pulsed method using successive pulses of H_2/$TiCl_4$ obtained by opening and closing pneumatic valves at regular intervals through a programmable controller. A 'pulse' is composed of an injection stage of gases into the reactor, a reaction stage with the gases in the closed reactor and an evacuation stage of the gases by the pumping system [10, 12–14]. The injection, reaction and evacuation times were equal to 0.5, 4 and 3 s, respectively. A H_2/$TiCl_4$ gas supply tank was located upstream from the reactor to inject rapidly the gaseous mixture in it. The pressure of pulse reaction stages in the reactor was fixed by both the injection time and the supply tank pressure and was about 3 kPa. The dilution rate R was estimated with the following equation from steady state:

$$R \approx \frac{D_{H_2}}{D_{TiCl_4}} = \frac{P_{Tank} - P_{TiCl_4}}{P_{TiCl_4}}, \quad (2)$$

where P_{TiCl_4} is the vapour pressure of $TiCl_4$ at 293 K.

Here, the dilution rate R was about 12. The temperature of treatment was 1,373 K. The conversion rate of carbon into TiC was studied as a function of the number of

Table 1 Main parameters of synthesis of TiC coatings

	P-RCVD	AP-RCVD
Temperature (K)	1,373	1,323
Dilution rate (H_2/$TiCl_4$)	~12	~78
Working pressure (kPa)	~3	~100
Supply tank pressure (kPa)	~19	~100
Treatment time	–	From 30 to 60 min
Number of H_2/$TiCl_4$ pulses	From 20 to 100 pulses	–
Time of introduction (s)	0.5	–
Time of reaction (s)	4.0	–
Time of evacuation (s)	3.0	–

Table 2 Deposition parameters and mechanical results obtained for the fibres treated by P-RCVD at 1,373 K

Batch label	Gas	Dilution rate	Working pressure (kPa)	Number of pulses	Stress at failure (MPa)	Standard deviation (MPa)
$\#Ti^{20p}$	$H_2/TiCl_4$	12	3.2	20	1,800	400
$\#Ti^{40p}$	$H_2/TiCl_4$	12	3.4	40	1,100	200
$\#Ti^{60p}$	$H_2/TiCl_4$	12	3.4	60	560	300
$\#Ti^{100p}$	$H_2/TiCl_4$	12	4	100	Brittle behaviour	–
$\#H^{100p}$	H_2	–	4	100	2,600	900
$\#Ti^{f40p}$	$H_2/TiCl_4$	12	2	40	1,800	700

$\#Ti^{-p}$ and $\#H^{100p}$ correspond to fibres coated with an initial porous carbon coating while $\#Ti^{f40p}$ without an initial porous carbon coating

Table 3 Deposition parameters and mechanical results obtained for the fibres with an initial porous carbon coating treated by AP-RCVD at 1,323 K

Batch label	Gas	Dilution rate	Treatment time (min)	Stress at failure (MPa)	Standard deviation (MPa)
$\#Ti^{30min}$	$H_2/TiCl_4$	78	30	1,600	300
$\#Ti^{48min}$	$H_2/TiCl_4$	78	48	500	100
$\#Ti^{60min}$	$H_2/TiCl_4$	78	60	Brittle behaviour	–

$H_2/TiCl_4$ pulses (20, 40, 60 and 100). Table 2 lists the P-RCVD parameters for each batch of treated fibres.

In the AP-RCVD variant, the gaseous mixture flowed continuously at a constant rate and atmospheric pressure in the open reactor heated at 1,323 K. The dilution rate calculated from equation [2] was about 78. The conversion of the initial porous layer was studied by varying the treatment time between 30 and 60 min. Table 3 lists the AP-RCVD parameters for each batch of treated fibres.

Characterisation of coatings

Chemical analyses of coatings were carried out by Auger electron spectroscopy (AES-VG Microlab 310F spectrometer) with simultaneous Ar^+ etching in order to obtain the concentration depth profiles of carbon, titanium, oxygen and silicon. The Auger spectra were obtained with an electron beam energy of 10 kV and a beam current of 5 nA and focused to a spot on substrate (about 1 μm). For the etching, the voltage and current of the ion beam were kept at 4.0 kV and 0.5 μA, respectively. The sputtering rate was estimated at 1 Å/s. X-ray photoelectron spectroscopy (XPS) was used to determine the chemical bonds in which these chemical elements are involved. XPS spectra were acquired with a VG Escalab 220i XL spectrometer using a monochromatized AlKα X-ray source (1486.6 eV) at 70 W and 40 eV pass energy. The diameter of the fibre was about 14 μm and the X-rays spot size was around 200 μm in diameter. Ar^+ sputtering was performed with an estimated etching rate of 0.3 nm/s. XPS spectra were fitted and quantified using the AVANTAGE software provided by Thermo Fisher Scientific. Coatings were observed by scanning electron microscopy (SEM-Quanta 400 FEG V2 microscope) using backscattered electron (BSE) and secondary electron (SE) detectors, with an accelerating voltage fixed at 15 kV. The presence of titanium in the coating was checked by energy dispersive x-ray spectroscopy. The microstructural study was performed by transmission electron microscopy (TEM-Philips CM30 microscope) using a LaB_6 source operating at 300 kV. The TEM thin-foil samples were prepared using an Argon ion slicing method [15].

A specific table-model testing machine was used to perform tensile tests at room temperature. Fibre failure stresses were obtained from 20 tests per batch with a gauge length of 25 mm according to a single fibre test procedure [16]. The fibre was mounted on a paper frame; the paper frame was aligned in the grips and then the frame sides were cut. The fibre was loaded up to failure. The stresses at failure were determined by dividing the load at failure by the section of the fibre. For each batch, the given value was an arithmetic mean obtained from the 20 tested fibres.

Results

Structure

In P-RCVD mode

AES concentration depth profiles for the batch $\#H^{100p}$, $\#Ti^{20p}$ and $\#Ti^{40p}$ fibres are displayed in Fig. 1. As a general rule, when the etching time, i.e. the etching depth, increases, the carbon and silicon contents varies till they reach the same constant value meaning that the SiC-based fibre is reached.

The detected elements are carbon, oxygen and silicon for the batch $\#H^{100p}$ fibres treated with pure H_2 pulses at

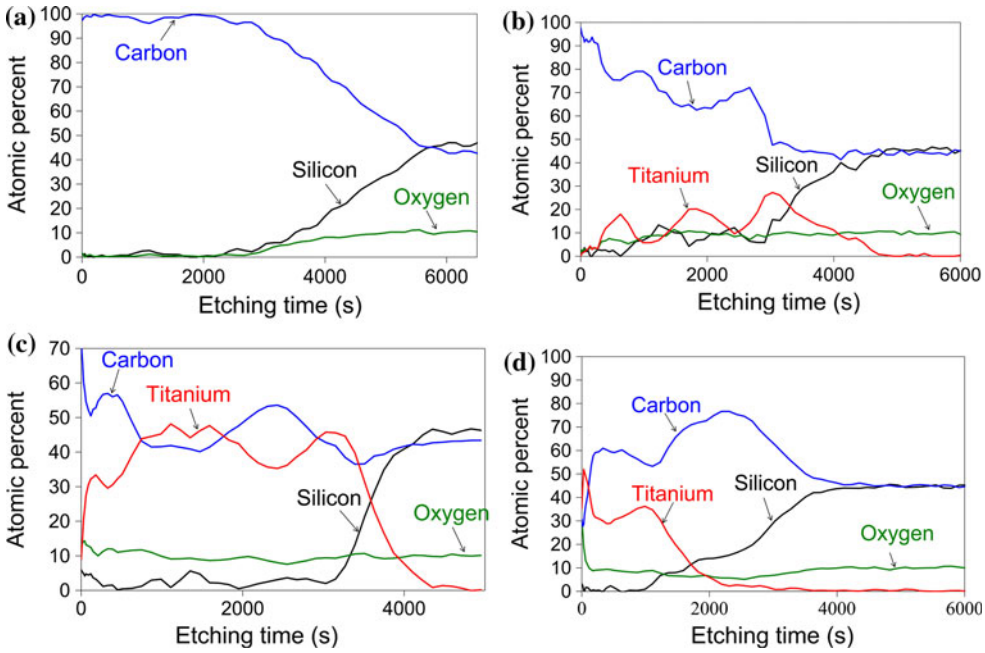

Fig. 1 Auger depth profiles of carbon, oxygen, titanium and silicon for (**a**) batch #H^{100p} fibre, (**b**) batch #Ti^{20p} fibre, (**c**) batch #Ti^{40p} fibre and (**d**) batch #Ti^{48min} fibre

1,373 K. No impurity is observed. The evolution of these elements as a function of depth is shown in Fig. 1a. Inside the porous coating, carbon content is higher than 99 at.% while oxygen content is lower than 0.6 at.%. The oxygen content increases gradually inside the fibre up to about 10 at.% which corresponds to the oxygen content of the NL 202 Nicalon fibre bulk [17].

The concentration depth profiles of carbon, oxygen, silicon and titanium for the batch #Ti^{20p} and #Ti^{40p} fibres treated with 20 $H_2/TiCl_4$ pulses and 40 $H_2/TiCl_4$ pulses at 1,373 K are shown, respectively, in Fig. 1b, c. Concerning the batch #Ti^{20p} fibre (Fig. 1b), carbon content decreases from about 98 at.% at the surface to about 47 at.% in depth whereas titanium content increases from 0 at the surface to 27 at.% at the fibre/modified coating interface with several oscillations. Concerning the batch #Ti^{40p} fibre (Fig. 1c), the carbon content, about 60 at.%, is higher at the surface than in depth, about 45 at.%, whereas titanium content is lower at the surface, about 8 at.%, than in depth, about 45 at.%. The $H_2/TiCl_4$ gases seem to react with the carbon situated in the bulk of the initial porous coating. Inside the modified carbon coating, the oxygen content is about 10 at.% for the batch #Ti^{20p} and #Ti^{40p} fibres (Fig. 1b, c) whereas it is detected in very low quantity for the batch #H^{100p} fibre (Fig. 1a). The presence of oxygen could result from thermal diffusion from the bulk of the fibre during the RCVD treatment or ambient air oxidation after the RCVD treatment.

Figure 2a–d shows the C1s and Ti2p XPS peaks for the batch #Ti^{40p} fibre at the surface and after 480 s etching, respectively. At the surface, without etching, the C1s spectrum reveals the main contribution of Csp^2 whereas the spectrum in Ti2p area hardly reveals a peak at 459 eV. This peak is very weak showing that there is almost not titanium at the surface and, consequently, the $Ti2p_{1/2}$ component peak is lost in the background noise. After 480 s etching, the fit of C1s peak shows the presence of carbon in the form of Csp^2, Csp^3 and carbon linked to oxygen (C–O, C=O, C–CO). Moreover, the fit reveals the contribution of the Ti–C bonding at 291.9 eV (TiC) and the contribution of oxycarbide at 282.9 eV. The Ti2p curve is composed of two mean peaks: $Ti2p_{3/2}$ (454–460 eV) and $Ti2p_{1/2}$ (460–465 eV). The fit of $Ti2p_{3/2}$ reveals the following types of phase bonding: Ti–C at 455.8 eV for carbide, Ti–O at 458.9 eV for TiO_2 and Ti(C*x*,O*y*) at 456.0 eV and Ti(C*y*,O*x*) at 455.8 eV with $x > y$ for intermediate oxides. The atomic rate of TiC, TiO_2 and intermediate oxides are 49, 9 and 42%, respectively. In depth, the analysis reveals that the carbon is linked not only to both carbon and oxygen but also to titanium, evidencing the formation of titanium carbide and titanium oxycarbide. The contribution of the Ti–C bonding increases with etching depth.

The XPS spectra of the batch #Ti^{f40p} fibre, i.e. the as-received fibre (without an initial porous carbon coating) directly treated with 40 $H_2/TiCl_4$ pulses, is shown in Fig. 2e, f. The fit of the spectra C1s shows the main contributions of Csp^2 and Csp^3 and carbon linked to oxygen. The presence of both Ti–C and Ti–C–O bonds is also observed. The Ti2p spectrum confirms the presence of TiC (57%), Ti(C*x*,O*y*) (27%) and TiO_2 (16%). The presence of titanium carbide and oxycarbide can result either from a direct solid–gas reaction between $H_2/TiCl_4$ and the fibre surface or a reaction between $H_2/TiCl_4$ and species produced by the thermal decomposition of the fibre.

Figure 3 shows BSE SEM images of the modified carbon coating obtained for batch #Ti^{20p}, #Ti^{40p} and #Ti^{100p}

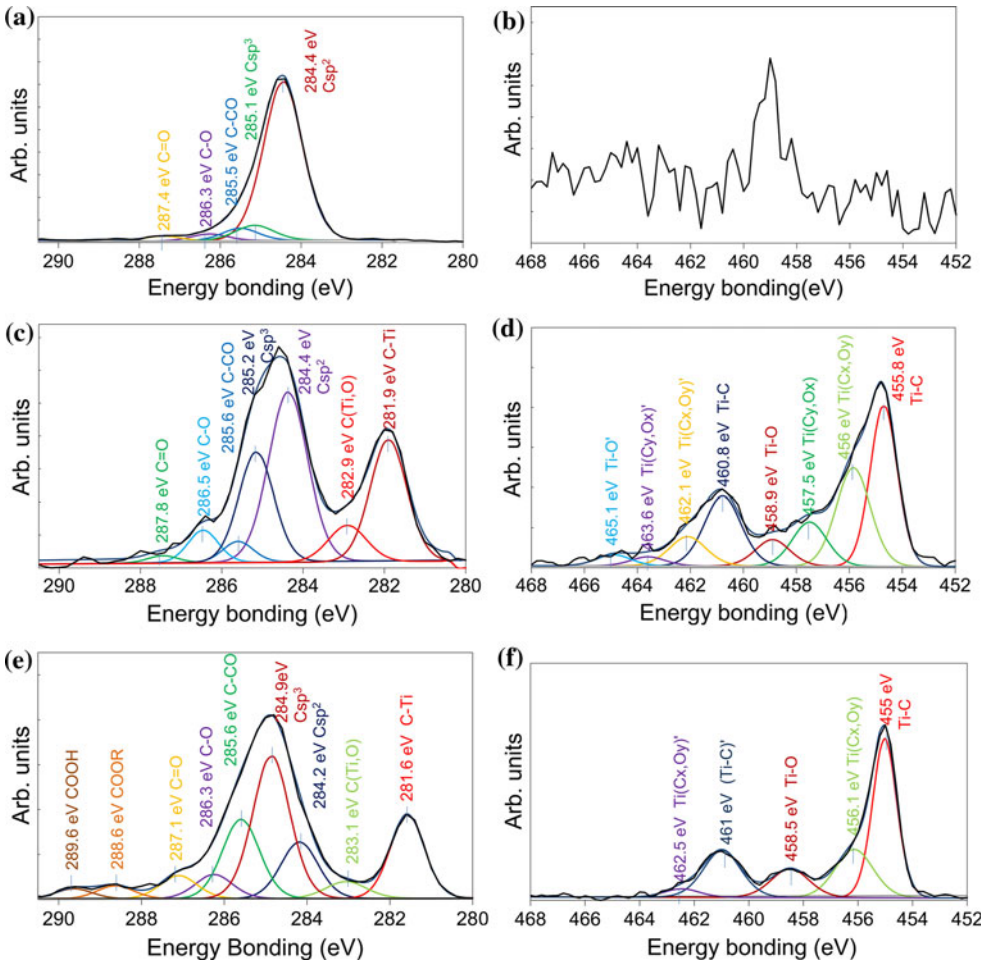

Fig. 2 C1s and Ti2p XPS spectra for batch #Ti^{40p} (**a**, **b**) at the surface of the modified porous carbon coating and (**c**, **d**) after etching of 480 s and for batch #Ti^{f40p} (**e**, **f**) at the surface of the fibre

fibres treated with 20, 40 and 100 $H_2/TiCl_4$ pulses, respectively. The uniformity of the treatment and the conversion rate inside the coating can be assessed through BSE images, where the observed bright areas are linked to titanium owing to its higher atomic number. The presence of titanium is confirmed by EDS. For 20 $H_2/TiCl_4$ pulses (Fig. 3a), bright scattered spots inside the coating and a white continuous interlayer at the fibre/modified carbon coating interface with a thickness of about 20 nm are observed. A white outer discontinuous layer is also observed at the surface of the porous carbon coating. With 40 $H_2/TiCl_4$ pulses (Fig. 3b), the coating is partially bright. The interlayer at the fibre/modified carbon coating interface is still present and is thicker than with 20 pulses, about 35 nm instead of 20 nm. Inside the modified porous carbon coating, a dark carbon-rich area is observed near the interface. This area can be linked to the increase of the carbon content observed as a small peak in the centre of the AES profile in Fig. 1c. As a general rule, the conversion rate clearly increases with the number of $H_2/TiCl_4$ pulses. The initial coating is totally converted with 100 $H_2/TiCl_4$ pulses (Fig. 3c). The presence of the isolated carbide grains within the porous carbon layer explains the oscillations observed in Auger depth profiles (Fig. 1). These oscillations decrease when the number of $H_2/TiCl_4$ pulses increases. Hence, the titanium amount in sample #Ti^{40p} (Fig. 1c) oscillates less than in sample #Ti^{20p} (Fig. 1b) and tends to a constant value equal to the carbon amount because the density of these carbide grains increases with the RCVD treatment. In both cases (Fig. 1b, c), it can be noted that after the oscillations, the Ti content passes through a maximum at around 3,000 s corresponding to the continuous TiC interlayer present in the surface of the fibre and then decreases from that maximum to zero at around 4,500 s when the fibre bulk composition is reached. The formation of TiC occurs not only inside the coating (as evidenced by the presence of the scattered spots in the BSE images), but also especially at the interface between the initial porous carbon coating and the fibre (giving rise to the formation of the interlayer). The $TiCl_4$ gas has diffused through the whole porous carbon coating reacting slightly within it and considerably at the interface with the fibre.

Figure 4 shows TEM cross-section micrographs. Figure 4a shows the carbon coating partially modified by

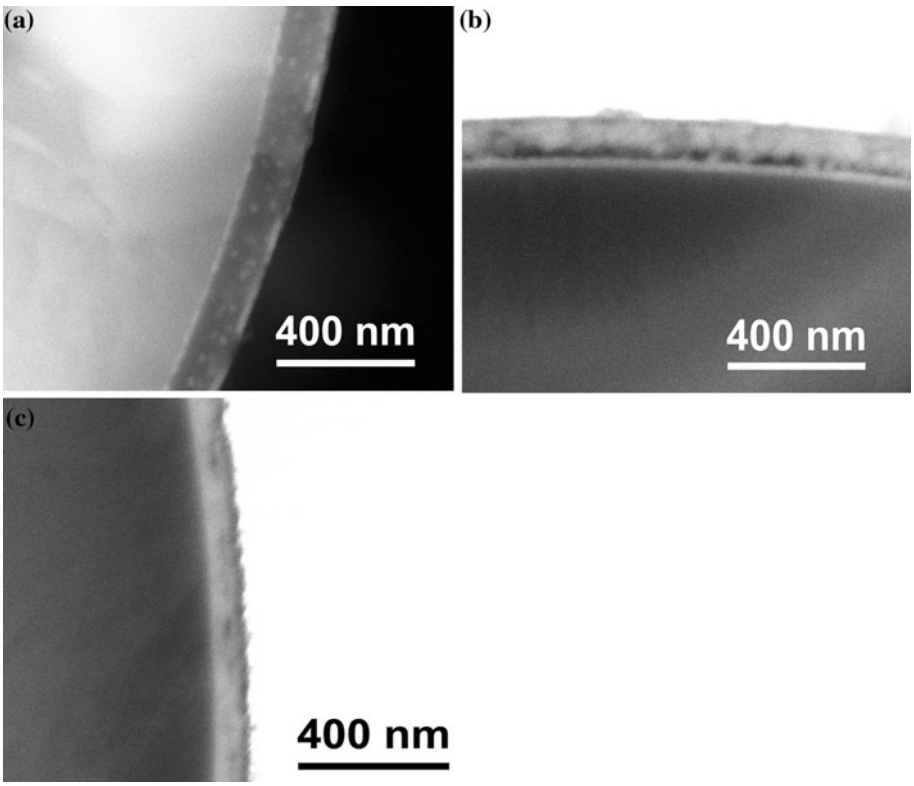

Fig. 3 BSE SEM images for (**a**) batch #Ti^{20p} fibre, (**b**) batch #Ti^{40p} fibre and (**c**) batch #Ti^{100p} fibre obtained in the P-RCVD mode

the treatment with 40 $H_2/TiCl_4$ pulses, e.g. batch #Ti^{40p} fibre. This coating is made of three layers. (i) An outer layer which is discontinuous and in which well-crystallised areas are observed. In this layer, the interplanar spacing measured from the lattice image is 0.249 nm, which agrees with the (111) interplanar spacing of TiC. These results confirm those of XPS analysis showing the presence of titanium carbide. (ii) An intermediate layer which is made of carbon mainly in the amorphous form and scattered TiC grains. (iii) An inner continuous layer at the fibre surface which is made of TiC.

Figure 4b shows the carbon coating entirely modified by the treatment with 100 $H_2/TiCl_4$ pulses, e.g. batch #Ti^{100p} fibre. The coating presents many microcracks perpendicular to the surface of the fibre. These can result from the contraction of the coating during the cooling stage at the end of the RCVD treatment as a consequence of the thermal expansion mismatch between SiC and TiC. It should be noted that the preparation of the thin foil for TEM combined with the high brittleness of the coating can also enhance microcracks. In any case, the visible shrinkage does not account for a possible conservation of the initial coating porosity. Furthermore, a serrated interface is observed on the fibre side. These damaged areas at the interface may result from a fibre chemical attack by the chlorinated gases. The gases would go across the coating and react with the elements of the fibre. This gaseous diffusion could be favoured by the presence of the microcracks.

In AP-RCVD mode

Figure 1d shows the AES concentration depth profiles for batch #Ti^{48min} fibre treated with $H_2/TiCl_4$ gas for 48 min. Carbon content increases from about 30 at.% at the surface to about 77 at.% at the coating/fibre interface whereas titanium content decreases from 50 at.% at the surface to about 1 at.% at the coating/fibre interface. Contrary to the titanium content, the carbon content is higher in depth than at the surface. The $H_2/TiCl_4$ gas seems to react preferentially with the carbon coating at the surface.

Figure 5 shows the SEM images (BSE and SE) of the modified coating for batch #Ti^{30min} fibre and batch #Ti^{48min} fibre. For the treatment of 30 min (Fig. 5a), two areas are observed: an outer bright layer with high titanium content (confirmed by EDS) and an inner dark layer with high carbon content. About one-third in thickness of the initial porous carbon layer is converted into TiC on the outer side. No intermediate continuous interlayer at the carbon coating/fibre interface is observed but only some isolated TiC grains are noticed at the surface of the fibre. A reaction between the $H_2/TiCl_4$ gaseous mixture and the carbon of the initial layer may occur occasionally in depth. Thus, the treatment at atmospheric pressure is not homogeneous. For the treatment of 48 min, two layers are also observed in the BSE image (Fig. 5b), a bright outer one and a dark inner one. Both have roughly the same thickness, approximately 100 nm each. In the corresponding SE image (Fig. 5c), distinct

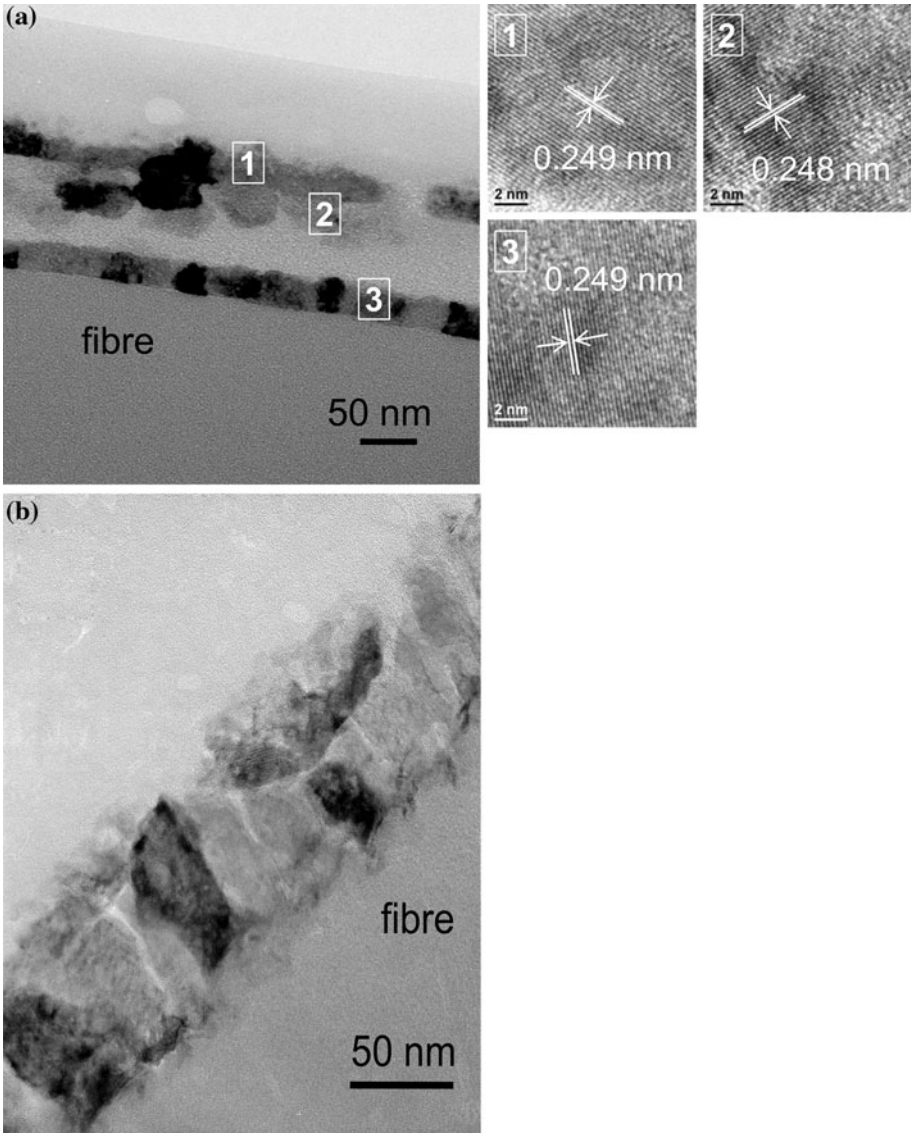

Fig. 4 TEM images for (**a**) batch #Ti^{40p} fibre and (**b**) batch #Ti^{100p} fibre obtained in the P-RCVD mode

morphologies are observed between the carbon coating and the converted coating. The conversion rate increases from one-third for 30 min of treatment to half for 48 min of treatment. For a treatment time of 60 min corresponding to the batch #Ti^{60min} fibre, the coating is entirely converted.

Figure 6 shows TEM images for the batch #Ti^{48min} fibre. As shown by SEM, an upper continuous layer is observed with a thickness of about 50 nm. This one is made of TiC (confirmed by electron diffraction). The presence of some individual grains at the surface of the fibre is observed. At high magnification, the measured interplanar spacing is 0.248 nm. As in the pressure-pulsed case, this one can be assigned to the (111) interplanar distance of TiC. These observations indicate that some H_2–$TiCl_4$ gas molecules go across the porous carbon coating. Nevertheless, compared with the P-RCVD case, this diffusion is limited and only few gaseous molecules react at the fibre surface.

Mechanical properties

The mean values of tensile stress at failure of the fibre batches obtained by P-RCVD and AP-RCVD are shown in Tables 2 and 3, respectively.

The stress at failure value of fibres with a porous carbon coating is about 3,100 MPa. This value is close to the one of the NL202 Nicalon fibre reported in the literature, about 3,000 MPa [17]. The presence of the porous carbon coating of 200 nm in thickness at the surface of the fibre has almost no influence on mechanical properties.

When the fibres (batch #H^{100p} fibres) are treated with 100 H_2 pulses at 1,373 K, the stress at failure is equal to about 2,600 MPa. The decrease of 500 MPa would be due to the thermal damage of the NL202 Nicalon fibre. There is an outgassing of oxides from the fibre such as SiO and CO and formation of flaws at the surface of the fibre [17].

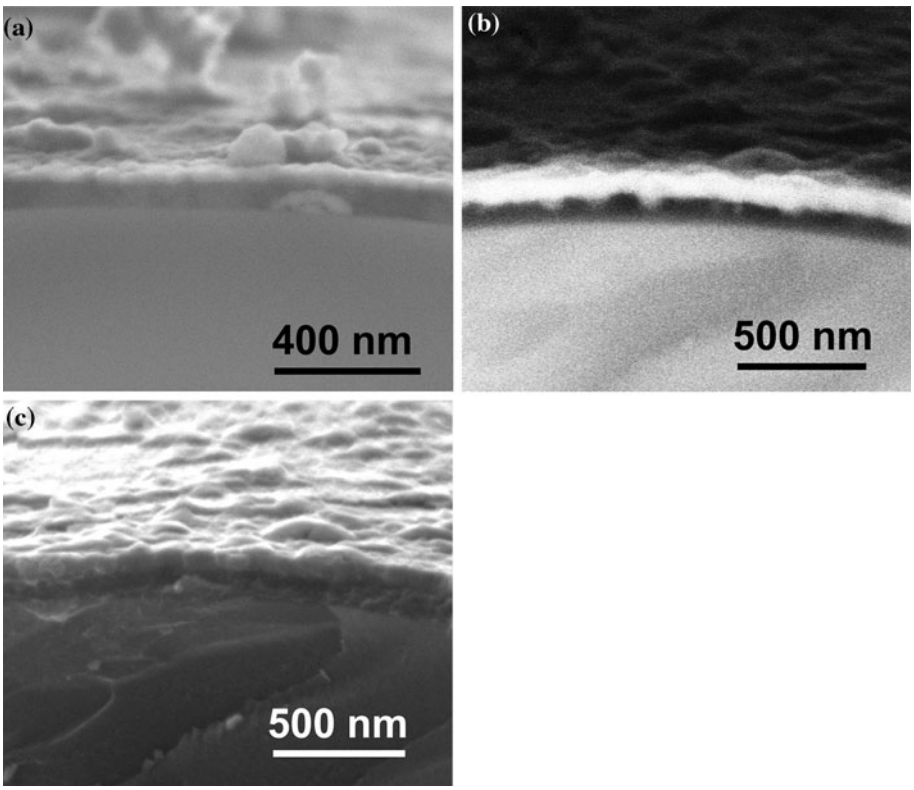

Fig. 5 BSE SEM images for (**a**) batch #Ti^{30min} fibre, (**b**) batch #Ti^{48min} fibre and SE SEM image for (**c**) batch #Ti^{48min} fibre obtained in the AP-RCVD mode

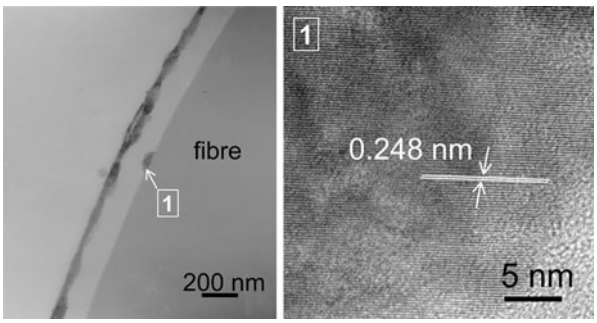

Fig. 6 TEM images for batch #Ti^{48min} fibre obtained in the AP-RCVD mode

Concerning the NL202 Nicalon fibres (batch #Ti^{f40p} fibres) without an initial porous carbon coating at its surface, the average stress at failure is about 1,800 MPa. Compared to batch #H^{100p} fibres, the stress at failure is decreased by 800 MPa. This strong decrease would be due to a chemical reaction between the $TiCl_4$ chlorinated gas and the fibre.

In P-RCVD, the stresses at failure decrease drastically with increasing number of $H_2/TiCl_4$ pulses. After 60 pulses, the fibre strength is only 560 MPa. For #Ti^{100p} fibres where the initial porous carbon coating is entirely converted, the stress at failure could not be determined because of the very low tensile strength of the fibres. The presence of a brittle (TiC) coating on direct contact with the surface of the fibre leads to the fibre strength fall.

In AP-RCVD, with the treatment of 60 min where the coating is entirely converted into brittle TiC, the fibre has a brittle behaviour. As in P-RCVD, no beneficial effect of a possible porosity in TiC is observed. However, surprisingly for shorter treatment times in atmospheric pressure, the fibre strength also decreases strongly with increasing treatment time, even though the TiC formation occurs preferentially on the outer carbon layer side.

Discussion

The synthesis of TiC is performed by converting the porous carbon coating at the surface of the fibre into a TiC coating by both P-RCVD and AP-RCVD with a $H_2/TiCl_4$ gaseous mixture. The conversion rate increases with the increasing number of pulses (P-RCVD) or treatment time (AP-RCVD). TiC continuous coatings are obtained with 100 $H_2/TiCl_4$ pulses by P-RCVD or with a treatment of 60 min by AP-RCVD. Nevertheless, the mode of conversion is different between the two methods. The involved mechanisms such as the diffusion of gases inside the porous carbon coating and the chlorinated gas ability to react with the carbon coating are not the same and are mainly connected to the working pressure and to the rate of dilution in hydrogen.

In P-RCVD, an interlayer is observed by SEM (Fig. 3a) at the surface of the fibre as soon as only 20 $H_2/TiCl_4$ pulses are used, i.e. the start of the treatment. This layer is made up

of TiC grains as confirmed by electron diffraction. Its thickness increases with the number of $H_2/TiCl_4$ pulses. The porous carbon layer is not very reagent towards the $H_2/TiCl_4$ gaseous mixture. Therefore, the gaseous species diffuse inside the porous carbon coating and react preferentially at the fibre–carbon coating interface. The reaction between the carbon and the $H_2/TiCl_4$ gaseous mixture near the fibre or in depth could be enhanced by the oxygen of the fibre and the presence of porosity in the carbon coating at the surface of the fibre. During the treatment at high temperature, the oxygen of the Nicalon fibre is evacuated in the form of instable gaseous species such as CO (g) and SiO (g) [17]. These instable gases would be thus confined to the porous carbon coating and would act as catalysts for the formation of titanium carbide in depth and more especially at the fibre surface (Fig. 3b). This would explain the presence of the TiC interlayer at the porous carbon coating–fibre interface and TiC scattered grains inside the carbon coating. It can be noted that the formation of CO (g) can also be enhanced by the reaction of $TiCl_4$ or/and the HCl by-product with the Nicalon fibre. To form the TiC interlayer, the carbon may also come from the fibre. Indeed, when the as-received fibre is directly treated with 40 $H_2/TiCl_4$ pulses at 2 kPa ($\#Ti^{f40p}$), a TiC layer with a thickness lower than 50 nm is formed at the surface of the fibre. This result shows that the fibre can react with the chlorinated gases. At this point, it is difficult to determine the origin of the carbon combined with titanium in the interlayer. It can be shown in Fig. 3b that an external discontinuous layer is also formed near the outer surface of the carbon coating. This discontinuous layer, where TiC grains are more concentrated than more in depth, may result from a graded gaseous reactant concentration in the porosity of the carbon layer. Nevertheless, the moderated depletion of the infiltrated precursor gas does not prevent the formation of the inner interlayer where the reaction is catalysed. In order to study the influence of the fibre chemical composition, a further treatment with 40 $H_2/TiCl_4$ pulses at 1,373 K has been performed on a porous carbon coating obtained at the surface of Hi-Nicalon fibres (Nippon Carbon), i.e. oxygen-free SiC-based fibres of second generation. A white outer discontinuous layer of 80 nm in thickness is observed (Fig. 7). Contrary to the treatment with NL202 Nicalon fibres ($\#Ti^{20\text{-}40p}$ fibre), the conversion of C into TiC starts only at the surface of the porous carbon coating. No interlayer at the carbon coating/fibre interface is observed. This difference can be linked to the oxygen content in the fibres, about 12 at.% for the NL202 Nicalon fibre and only about 0.6 at.% for the Hi-Nicalon fibre [17, 18]. The Hi-Nicalon fibre is stable up to 1,673–1,773 K. No or little gaseous species are formed at 1,373 K. Therefore, in the case of the Nicalon fibre, the instable species such as CO (g) or SiO (g)

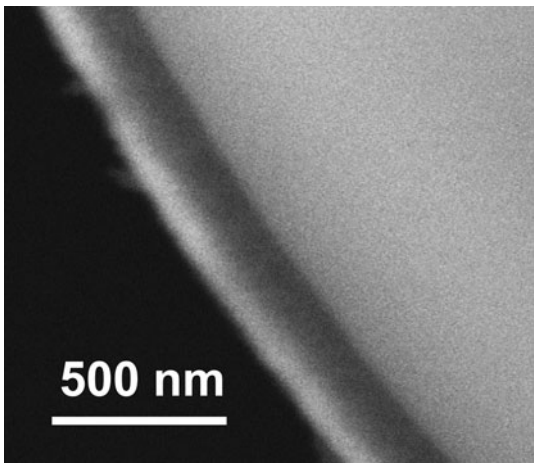

Fig. 7 BSE SEM image of the modified porous carbon coating at the surface of a Hi-Nicalon fibre treated with 40 $TiCl_4/H_2$ pulses at 1,373 K

would play an important role in the activation of the reaction between the carbon and $H_2/TiCl_4$.

In AP-RCVD, the used dilution rate is about 78 (instead of 12 in P-RCVD). Therefore, the partial pressure of $TiCl_4$ is five times as big, about 1.3 kPa, as in AP-RCVD, about 0.25 kPa. Because of the simultaneous increase of $TiCl_4$ partial and total pressure, the ability of the $H_2/TiCl_4/C$ system to react is better in AP-RCVD than in P-RCVD in spite of the decrease of the temperature to 1,323 K. As shown by the AES analysis (Fig. 1d), the titanium content is higher at the outer surface than in depth in AP-RCVD unlike in P-RCVD. In AP-RCVD, the conversion begins at the external surface of the coating and continues in depth while in P-RCVD the conversion begins preferentially at the fibre–carbon coating interface and continues to the external surface of the coating. Hence, the diffusion of gaseous species is limited at high pressure.

As evidenced by the mechanical tests (see Table 2), the NL202 Nicalon fibre ($\#Ti^{f40p}$, without a porous carbon coating) is damaged by the formation of the TiC coating at its surface. The tensile strength of the fibre can be thus decreased due to a chemical attack by chlorinated gases and a notch effect induced by the presence of a strongly bonded brittle layer that leads to the existence of new surface flaws [19–22]. In the same manner for fibres initially coated with porous carbon and then treated by P-RCVD, the stress at failure decreases gradually as a function of the number of $H_2/TiCl_4$ pulses, i.e. with both the increase of the thickness of the TiC interlayer at the fibre surface and the increase of the carbon conversion rate. For the AP-RCVD method (see Table 3), the fibre strength also decreases dramatically with increasing treatment time even though a continuous brittle TiC interlayer is not observed at the interface between the fibre surface and the initial porous carbon coating. This

decrease can be explained by the inhomogeneity of the treatment at atmospheric pressure, as shown by the presence of some isolated TiC grains scattered at the surface of fibre in Fig. 5a. This presence that could not be totally prevented by the use of the atmospheric pressure method also initiates new surface flaws that are as detrimental to the fibre strength as a continuous brittle carbide layer.

Conclusion

Porous carbon coatings at the surface of SiC-based fibres have been converted into titanium carbide coatings by RCVD with a $H_2/TiCl_4$ gaseous mixture both in the pressure-pulsed mode and the atmospheric pressure mode. After total carbon conversion, the resulting titanium carbide coating is shrunk and carbide porosity could not be pointed out. In both modes, when the treatment time (or the number of pulses for P-RCVD) increases, the conversion rate of the porous carbon coating increases and the mechanical properties of the fibres decrease. The obtained low values of the stress at failure can be explained by the attack of $H_2/TiCl_4$ gases on the elements of the fibre and by the presence of brittle TiC at the surface of the fibre either in the form of a continuous layer for P-RCVD or isolated grains for PA-RCVD.

Acknowledgements We would like to thank J. L. Leluan, J. Thebault and S. Bertrand from SPS and J.-D. Lulewicz from CEA.

References

1. Pichon T, Barreteau R, Soyris P, Foucault A, Parenteau JM, Prel Y, Guedron S (2009) Acta Astronaut 65:165
2. Bhatt RT, Choi SR, Cosgriff LM, Fox DS, Lee KN (2008) Mater Sci Eng A 476(1–2):20
3. Naslain R (1998) Composites A 29A:1145
4. Carpenter HW, Bohlen JW, Steffier WS (1992) US Patent No. 5,221,578
5. Holmquist M, Lundberg R, Sudre O, Razzell AG, Molliex L, Benoit J, Adlerborn J (2000) J Eur Ceram Soc 20:599
6. Nubian K, Saruhan B, Kanka B, Schmücker M, Schneider H, Wahl G (2000) J Eur Ceram Soc 20:537
7. Jacques S, Rapaud O, Parola S, Verdenelli M (2005) Ann Chim 30(6):609
8. Gogotsi Y, Jeon I, McNallan MJ (2003) Ceram Eng Sci Proc 24(3):57
9. Piquero T, Vincent H, Vincent C, Bouix J (1995) Carbon 33(4): 455
10. Rapaud O, Jacques S, Di-Murro H, Vincent H, Berthet M-P, Bouix J (2004) J Mater Sci 39:173. doi:10.1023/B:JMSC.0000007742.34926.65
11. Delcamp A, Maillé L, Saint Martin S, Pailler R, Guette A (2010) Comp Sci Technol 70(4):622
12. Dupel P, Bourrat X, Pailler P (1995) Carbon 33(9):1193
13. Heurtevent F (1996) PhD thesis no 1476. University of Bordeaux-1, France
14. Naslain R, Pailler R, Bourrat X, Bertrand S, Heurtevent F, Dupel P, Lamouroux F (2001) Solid State Ionics 141–142:541
15. Weisbecker P, Guette A (2009) In: Proceedings of 17th international conference on composite materials, 27:D3:1, ICCM 17, Edinburgh
16. Lamon J, Rechiniac C, Lissart N, Corne P (1992) In: Bunsell AR, Jamet JF, Massiah A (eds) Proceedings of the 5th European conference on composite materials, Bordeaux, France (EACM-CEC, Paris, Bordeaux, 1992), pp 895–900
17. Pailler R, Lamon J, Guette A, Sauder C, Martin-Litas I (2005) Ann Chim 30(6):565
18. Bunsell AR, Berger M-H (2000) J Eur Ceram Soc 20:2249
19. Ochiai S, Murakami Y (1979) J Mater Sci 14:831. doi:10.1007/BF00550714
20. Ochiai S, Osamura K, Honjo K (1992) Mater Sci Eng A 154:149
21. Bertrand P, Vidal-Sétif M-H, Valle R, Mévrel R (1998) J Mater Sci 33(20):5029. doi:10.1023/A:1004467226248
22. R'Mili M, Massardier V, Merle P, Vincent H, Vincent C (1999) Carbon 37:129